Genes & Diseases (2022) 9, 252–267

Available online at www.sciencedirect.com

ScienceDirect

journal homepage: http://ees.elsevier.com/gendis/default.asp

FULL LENGTH ARTICLE

PTEN and AKT/GSK-3β/CRMP-2 signaling pathway are involved in neuronal apoptosis and axonal injury in early brain injury after SAH in rats

Hong Chen [a], Chao Zhou [a], Jianfeng Zheng [a], Zhaosi Zhang [a], Yongbing Deng [b], Chongjie Cheng [a], Zongduo Guo [a], Gang Huo [a], Cheng Yin [c,**], Xiaochuan Sun [a,*]

[a] *Department of Neurosurgery of the First Affiliated Hospital of Chongqing Medical University, Chongqing 400016, PR China*
[b] *Department of Neurosurgery of the Chongqing Emergency Medical Center, Chongqing 400014, PR China*
[c] *Department of Neurosurgery, Sichuan Provincial People's Hospital, University of Electronic Science and Technology of China, Chengdu, Sichuan 610072, PR China*

Received 5 March 2020; received in revised form 16 April 2020; accepted 7 May 2020
Available online 18 June 2020

KEYWORDS
AKT/GSK-3β/CRMP-2 pathway;
Axonal injury;
Early brain injury;
Neuronal apoptosis;
PTEN;
Subarachnoid hemorrhage

Abstract In early brain injury (EBI) after subarachnoid hemorrhage (SAH), white matter (WM) axonal injury plays a key role in the prognosis of the disease. The purpose of this study was to investigate the effects of phosphatase and tensin homolog deleted on chromosome ten (PTEN) on axonal injury and neuronal apoptosis post-SAH in rats and to find its underlying mechanism. Adeno-associated virus was injected into the lateral ventricle to suppress or promote PTEN. Neural function post-SAH in animals was determined by the modified Garcia score, beam balance, and Rotarod test, and the blood–brain barrier disruption was assessed by the brain water content. Axonal injury post-SAH was observed by TEM and determined by IF, and neuron apoptosis was measured by TUNEL staining. The mechanism was analyzed by Western blot to detect p-PTEN/PTEN, p-AKT/AKT, p-GSK-3β/GSK-3β, p-CRMP-2/CRMP-2, axonal injury marker β-APP and pro- and anti-apoptosis proteins, including Bax and Bcl-2, expression. We found 1. After knocking down PTEN, neuronal apoptosis and axonal injury were alleviated, and nerve function and blood–brain barrier were protected; accordingly, after overexpression

* Corresponding author. Department of Neurosurgery of the First Affiliated Hospital of Chongqing Medical University, Chongqing 400016, PR China.
** Corresponding author. Department of Neurosurgery, Sichuan Provincial People's Hospital, University of Electronic Science and Technology of China, Chengdu, Sichuan 610072, PR China.
E-mail addresses: yincheng@med.uestc.edu.cn (C. Yin), sunxch1445@qq.com (X. Sun).
Peer review under responsibility of Chongqing Medical University.

https://doi.org/10.1016/j.gendis.2020.05.002

of PTEN, neuronal apoptosis and axon damage were aggravated, and nerve function damage and blood—brain barrier damage were increased. 2. PTEN and AKT/GSK-3β/CRMP-2 pathway were jointly involved in regulating neuronal apoptosis and WM axon injury after SAH. According to our research, PTEN was a negative factor of EBI, and together with the AKT/GSK-3β/CRMP-2 signaling pathway aggravates neuronal apoptosis and WM axon damage after SAH. Inhibition of PTEN expression may become a new target for SAH treatment.

Introduction

Subarachnoid hemorrhage (SAH) is a fatal cerebrovascular disease with high morbidity and mortality.[1] Early brain injury (EBI) is an acute pathophysiological event within 72 h of bleeding and is considered to be the basis for the intervention and treatment of SAH patients.[2] White matter accounts for more than half of human brain tissue and is more susceptible to ischemic/hemorrhagic stroke than gray matter.[3] Beta-amyloid precursor protein (β-APP) is a cell surface protein that is transported along the axon.[4,5] The accumulation of β-APP is a sign that the rapid transport of axons is interrupted as a signal of axon injury.[6] It has been reported that neuronal apoptosis occurs in experimental SAH or in clinical patients after SAH.[7] Excessive neuronal apoptosis will aggravate the degeneration and damage of axons, resulting in dysfunction of axonal transport and axon-dendritic connection disorders.[8] Therefore, finding protective targets against neuronal apoptosis and WM axonal injury can greatly improve the therapeutic effect of SAH.

Phosphatase and tensin homolog deleted on chromosome ten (PTEN) is a tumor suppressor gene that is widely expressed in the central nervous system (CNS) of rats and plays a role in various neurological diseases.[9,10] Studies have reported that in experimental models of nerve injury, the inhibition of PTEN has the potential to protect axonal injury.[11,12] In a rat model of middle cerebral artery occlusion (MCAO), upregulation of PTEN expression can accelerate neuronal apoptosis.[13] Akt as a survival kinase prevents inflammation and apoptosis.[14] One of the most important downstream targets of Akt is the glycogen synthase kinase 3β (GSK-3β)/collapsin response mediator protein-2 (CRMP-2) pathway.[15] GSK-3β was originally identified as a negative regulator of glycogen metabolism, and it was later found that it can play a role in different cellular processes, including cell proliferation, differentiation, movement, and apoptosis.[16,17] CRMP-2 is related to neuron differentiation and axonal growth and plays an important role in the apoptosis and axonal contraction of dopaminergic neurons.[18,19] In neurons, GSK-3β is involved in neuronal microtubule dynamics, and GSK-3β inactivates CRMP-2 by phosphorylating it, causing axon/dendritic polarity disorder.[20] However, it is unclear whether the Akt/GSK-3β/CRMP-2 pathway is involved in axonal injury and neuronal apoptosis after SAH.

Our research wants to understand whether PTEN can aggravate neuronal apoptosis and axonal injury after SAH, and to explore whether Akt/GSK-3β/CRMP-2 signaling pathway is involved in this regulation.

Materials and methods

Experimental design

All experiments consisted of five parts. A detailed schematic of the experimental procedure and the location of the material were shown in the figure (Fig. 1A—C). All experiments were performed in a double-blind manner, and a randomized design was applied to all experiments.

Animals

The experimental animals were purchased from the Experimental Animal Center of Chongqing Medical University [Experimental Animal Production License: SCXK (Yu) 2018-0003; Laboratory Animal Use License: SYXK (Yu) 2018-0003]. Sprague—Dawley (SD) rats were housed in clean animal houses, provided sterile pellet feed and standard acidified water, and kept under 12 h light and dark conditions at 22 ± 0.5 °C and relative humidity of 55—60%. All experimental procedures were followed by the experimental animal operating procedures at Chongqing Medical University, and they were approved by the Animal Experimental Ethics Committee. A total of 224 adult male SD rats (body weight 280—330 g) were used for surgery and grouped by random. Detailed information about the rats is listed in Table 1.

SAH model

Experimental SAH was established by an intravascular perforation model as previously reported.[21] Briefly, rats were anesthetized with 3% sodium pentobarbital (30 mg/kg) by intraperitoneal injection. The adequacy of anesthesia depth was routinely observed by examining the pupil size and flexion reflexes. The left external carotid artery (ECA) and internal carotid artery (ICA) were exposed by a midline neck incision. The ICA was entered using a 4-0 monofilament nylon suture until resistance was detected. The nylon suture was then advanced approximately 3 mm to penetrate the bifurcation of the anterior cerebral artery

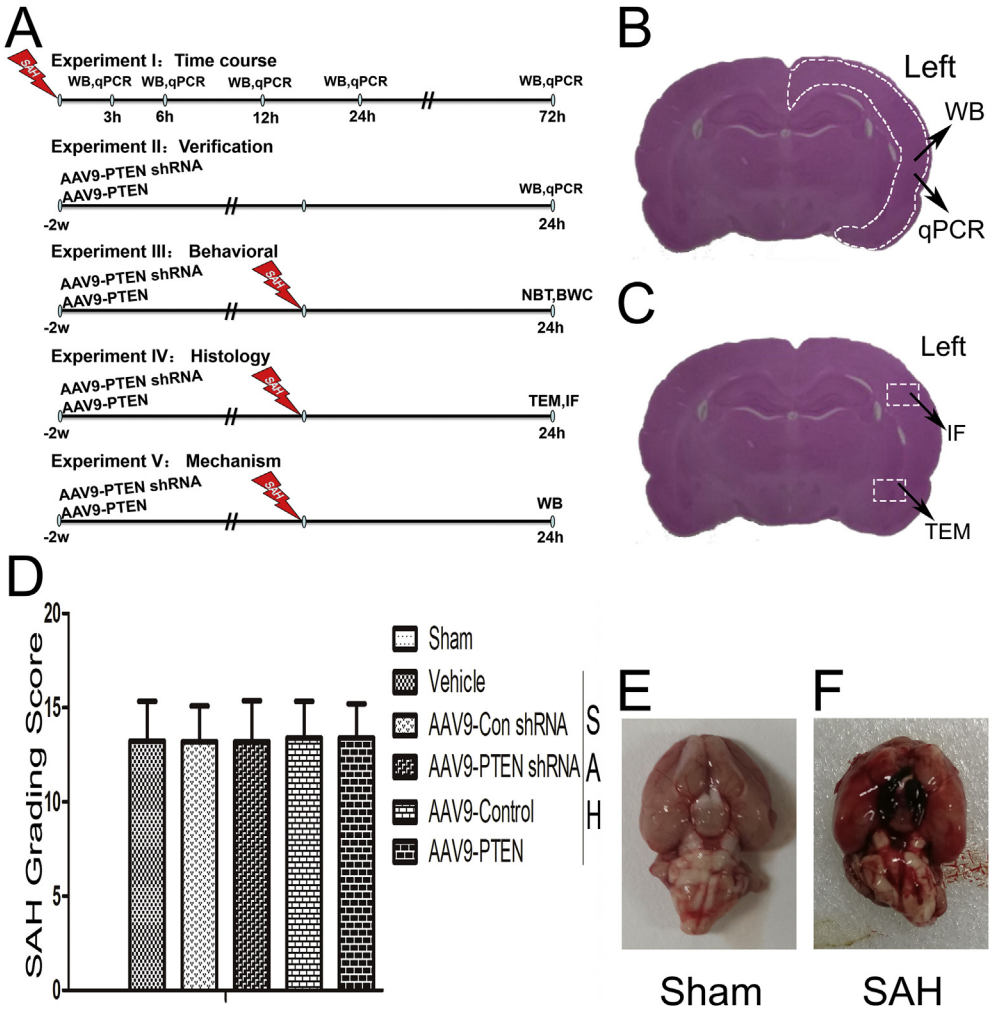

Figure 1 Basic experimental information and SAH grading scores of each group (NBT = Neurological behavioral test, BWC = Brain water content). (**A**) experimental design. (**B, C**) Sample area for each experiment. (**D**) SAH grading scores ($P > 0.05$). (E, F).

(ACA) and middle cerebral artery (MCA) and immediately withdrawn. In the sham group, all procedures except the vascular puncture were repeated. During the operation, the body temperature was maintained at 37.5 ± 0.5 °C with an electric blanket. Rats that died from severe SAH were replaced with rats from the same model to ensure that the experiment was complete.

SAH grading

The basal cistern was divided into six segments, each graded from 0 to 3 depending on the amount of blood clots.[22] The total score was calculated by adding all area scores (maximum SAH grade = 18). Eighteen rats with mild SAH (SAH grade ≤ 8) were excluded from the current study as previously described.

Adeno-associated virus preparation

The sequence design and virus preparation for all adeno-associated viruses were provided by Sangon Biotech (Shanghai, China). The serotype was AAV9, and the carrier was U6-MCS-CAG. The viral titer was determined by dot blot DNA analysis and expressed as a vector genome (vg/ml). The vector preparations used in this study showed a titer of 10^{12}-10^{13} vg/ml. Specific information is shown in Table 2.

Intraventricular rAAV vector delivery

Intracerebroventricular injection was operated as previously described.[23,24] SD rats receiving lateral ventricular injection were randomly divided into five groups: 1. AAV9-PTEN shRNA (knockdown group), 2. AAV9-Con shRNA (control virus for knockdown group), 3. AAV9-PTEN (overexpression group), 4. AAV9-Control (control virus for overexpression group), 5. Vehicle (physiologic saline, solvents for these viruses). The rats were anesthetized with sodium pentobarbital (30 mg/kg). A hole was drilled at the intersection of 1.5 mm outside the sagittal suture and 0.5 mm in front of the coronary suture. A 10 ml Hamilton syringe was fixed and inserted into the lateral ventricle 3.5 mm below the cortex, and then 10 μl of virus solution or saline was injected into the lateral ventricle at a rate of 0.5 ml/min. After the injection, the needle was left in

Table 1 The use of rats in different experiments in each group.

E	Groups	WB/PCR	NBT/BWC	IF/TEM	Death	Mortality (%)	Excluded
E1	Sham	5			0	0	0
	SAH (3 h,6 h,12 h,24 h,72 h)	39			9	23.08	5
E2	Nomal	5			0	0	0
	Nomal + AAV9-Con shRNA	5			0	0	0
	Nomal + AAV9-PTEN shRNA	5			0	0	0
	Nomal + AAV9-Control	5			0	0	0
	Nomal + AAV9-PTEN	6			1	16.67	0
E3	Sham		5		0	0	0
	SAH + Vehicle		5		0	0	0
	SAH + AAV9-Con shRNA		7		1	14.29	1
	SAH + AAV9-PTEN shRNA		6		1	16.67	0
	SAH + AAV9-Control		6		1	16.67	0
	SAH + AAV9-PTEN		10		3	30	2
E4	Sham			10	0	0	0
	SAH + Vehicle			13	2	15.38	1
	SAH + AAV9-Con shRNA			14	2	14.29	2
	SAH + AAV9-PTEN shRNA			13	2	15.38	1
	SAH + AAV9-Control			14	3	21.43	1
	SAH + AAV9-PTEN			17	5	29.41	2
E5	Sham	Shared with Experiment 1			0	0	0
	SAH + Vehicle	7			2	28.57	0
	SAH + AAV9-Con shRNA	7			1	14.29	1
	SAH + AAV9-PTEN shRNA	5			0	0	0
	SAH + AAV9-Control	7			1	14.29	1
	SAH + AAV9-PTEN	8			2	25	1

Table 2 Basic information about adeno-associated virus.

Gene	Species	Sequence	Gene_ID	Genbank
PTEN	Rat	(a) sense, GGUCAGCCGAGAGCAUCGUAAAGCA, antisense, UGCUUUACGAUGCUCUCGGCUGACC;	50557	NM_031606.1
		(b) sense, CACUGGUGGGUAAAGUAGCCAUCAC, antisense, GUGAUGGCUACUUUACCCACCAGUG;		NM_054382
		(c) sense, UUAAUAGUUUCGUGCAGCUACAUCU, antisense, AGAUGUAGCUGCACGAAACUAUUAA;		NM_0311306

place for 5 min and then slowly withdrawn to allow the fluid to fully diffuse into the cerebrospinal fluid (CSF). After surgery, the rats were allowed to eat freely, and experimental SAH surgery was performed 14 days later.

Quantitative analysis of PTEN mRNA knockdown and overexpression

AAV9-PTEN shRNA or AAV9-PTEN affects the expression level of PTEN mRNA in rat cortical tissue samples measured by quantitative real-time PCR (qRT-PCR). Tissue total RNA was extracted by the Trizol method, and cDNA was synthesized by reverse transcription. The PCR was carried out using cDNA as a template and a 10 μl reaction system, and the amplification conditions were as follows: predenaturation at 95 °C for 3 min; 95 °C for 10 s, 56 °C for 30 s, for a total of 40 cycles. Real-time PCR was applied with the following primers: forward primer: 5′-TGGATTC-GACTTAGACTTGACCT -3′ and reverse primer: 5′-GGTGGGTTATGGTCTTCAAAAGG-3′ for PTEN; forward primer: 5′- CACCCACTCCTCCACCTTTG′ and reverse primer:5′- CCACCACCCTGTTGCTGTAG-3′ for GAPDH. The dissociation curve was analyzed to confirm the specific amplification. The amplification of the overall cDNA samples were divided into 3 portions and standardized compared to a triplicate of GAPDH. The expression of the data was based on the $2^{-\Delta\Delta Ct}$ method as previously described.[25,26]

Neurological score

The neurological function of each group of rats was quantified by the modified Garcia neurological function scoring standard.[27,28] The autonomic activity, axial sensation, nasal

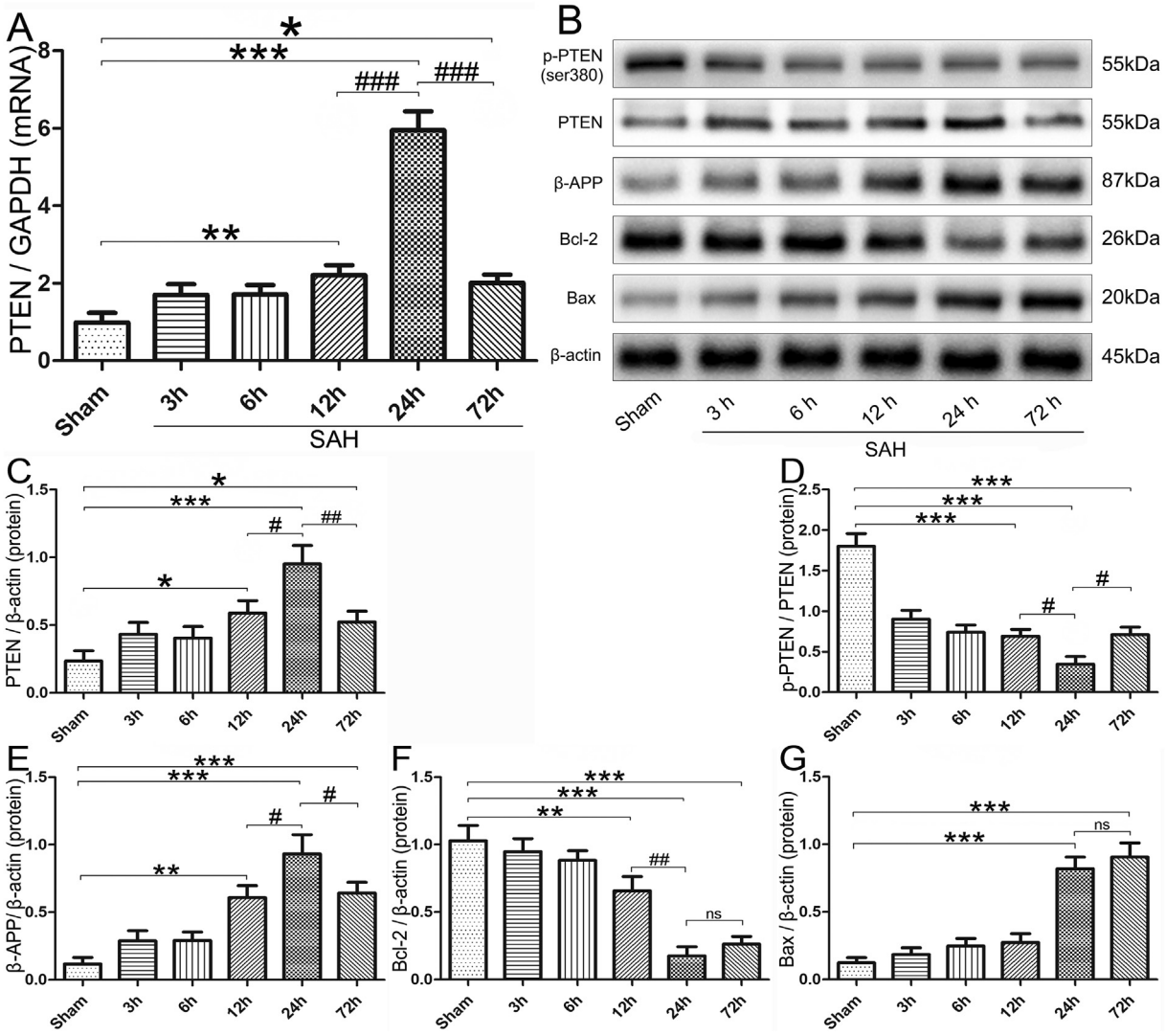

Figure 2 SAH increased PTEN, β-APP, and Bax and decreased p-PTEN and Bcl-2 in the left cortex at 24 h. **(A)** PTEN mRNA expression after SAH. **(B)** Western blot results. **(C—G)** Quantitative analysis of PTEN/(p-PTEN/PTEN)/β-APP/Bcl-2/Bax. Data were represented as the mean ± SD ($n = 5$ per group). (*P or $^{\#}P<0.05$, **P or $^{\#\#}P<0.01$, *vs.* ***P or $^{\#\#\#}P<0.001$,* means compared with the sham group; # means compared with the 24 h group; ns means no significant difference).

hair proprioception, limb extension, body lateral rotation and forelimb grip were recorded and scored. Each score accounted for 0 to 3 points, and the score ranged from 3 to 18 points. The higher the score, the milder the neurological dysfunction.

Rats were tested for motor integration and coordination by the balance beam experiment.[27,29,30] The scoring standard was based on the literature as follows: 0 points, and maintains a stable balance; 1 point, grasping one end of the balance beam; 2 points, clinging to the balance beam, one side of the limb slipping; 3 points, holding the balance beam, both sides of the body rotating around the wood Or fall (more than 60 s); 4 points, trying to maintain balance but slipping between 40 and 60 s; 5 points, trying to maintain balance but slipping between 20 and 40 s; 6 points, cannot maintain balance and sliding within 20 s.

Rota-rod latency

Motor function was measured by a Rota-rod (No 7750, Ugo Basile, Italy). The rats were trained twice for 10 min before surgery. First, the rats were accustomed to the fixed rod and then exposed to the runner. At the start, the speed was set at 4.5 rpm and then increased from 4.5 to 8 rpm. The measuring interval was more than 30 min, and the cut-off time was 300 s.[29,31] When the animal fell, the time was recorded. The measured value was defined as the average of three measurements.

Brain water content

At 24 h after operation, the rats in each group were deeply anesthetized by sodium pentobarbital. After perfusion with

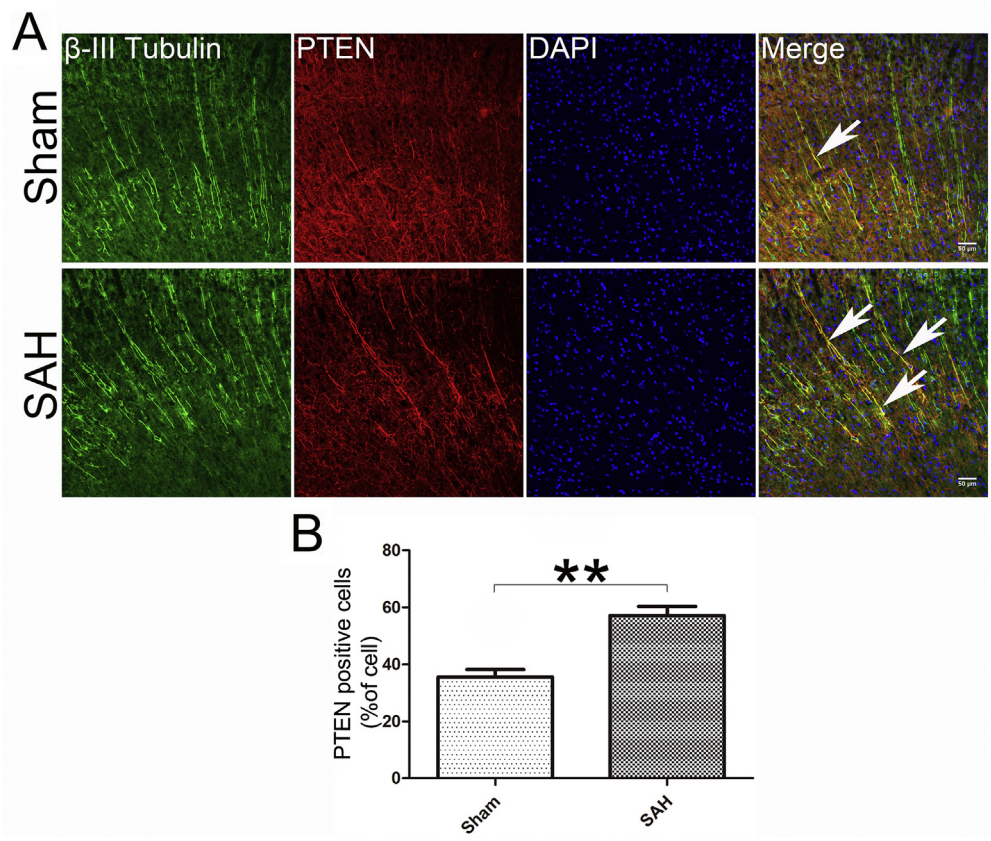

Figure 3 PTEN expression increased in the left cortex after SAH. **(A)** Expression of PTEN in the cortex and subcortical WM regions. **(B)** PTEN positive cell rate statistics. Data represent the mean ± SD ($n = 5$ per group). Student's *t*-test. (**$P<0.01$ *vs.* sham group). Scale bars, 50 μm.

saline at 4 °C, the head was quickly severed to obtain the entire brain, and the brainstem and cerebellum were quickly removed, the hemisphere tissue was separated and the wet weight was weighed. The brain tissue was placed in a 105 °C incubator for 72 h to constant weight, and the dry weight was determined. The percentage of brain water content was calculated as [(wet weight−dry weight)/wet weight] × 100%.

Transmission electron microscopy

At 24 h postoperative, the rats were deeply anesthetized and perfused with 0.9% saline and 2.5% glutaraldehyde. The dissected target brain tissues were fixed with 2.5% glutaraldehyde overnight, and ultrathin sections (60 nm) were made after fixing with gadolinium tetroxide for 2 h, dehydrated with acetone and stained with uranium acetate. All specimens were examined with electron microscope (Hitachi h-7000, Tokyo, JPN), and all images were analyzed using Northern Ecclestone Software (Cheektowaga, NY, USA).

Immunofluorescence staining

The rats were deeply anesthetized and perfused with 0.9% saline and 4% paraformaldehyde. The isolated brain was fixed in 4% paraformaldehyde for 24 h and dehydrated using sucrose (20%, 30%) for 24 h. Then, it was embedded in an OCT compound for cryosection and cut into 10 μm thick coronal sections. Next, fluorescent immunolabeling was performed according to the standard indirect technique as described previously. Primary antibodies used included PTEN (ab79156, 1:100, Abcam, Cambridge, MA, USA), β-APP (ab32136, 1:100, Abcam, Cambridge, MA, USA) and β III Tubulin (sc-51670, 1:200, Santa Cruz, Dallas, TX, USA). After washing three times in PBS, Dylight 488 conjugated Goat Anti-Rabbit IgG (A23220, 1:100, Abbkine, CA, USA) and Dylight 594 conjugated Goat Anti-Rat IgG (A23440, 1:100, Abbkine, CA, USA) were added to PBS containing 1% BSA for 1 h. In the final wash, 6-diamidino-2-phenylindole (DAPI) (28718-90-3, 1:100, Abbkine, CA, USA) was added and used as a counterstain for the nucleus. A ZEISS confocal laser scanning microscope was used to obtain fluorescence images (ZEISS LSM700, GER). $PTEN^{+}/\beta\text{-}APP^{+}$, in which positive cells were counted in 5 randomly selected regions (100×) of each slice using ImageJ software. Immunofluorescence staining was performed for five brains.

TUNEL staining

As reported in the literature,[32] brain samples were prepared 24 h after SAH. Apoptotic cells were detected by Annexin V-FITC Apoptosis Detection Kit (Sigma−Aldrich, Darmstadt, GER) and performed according to the

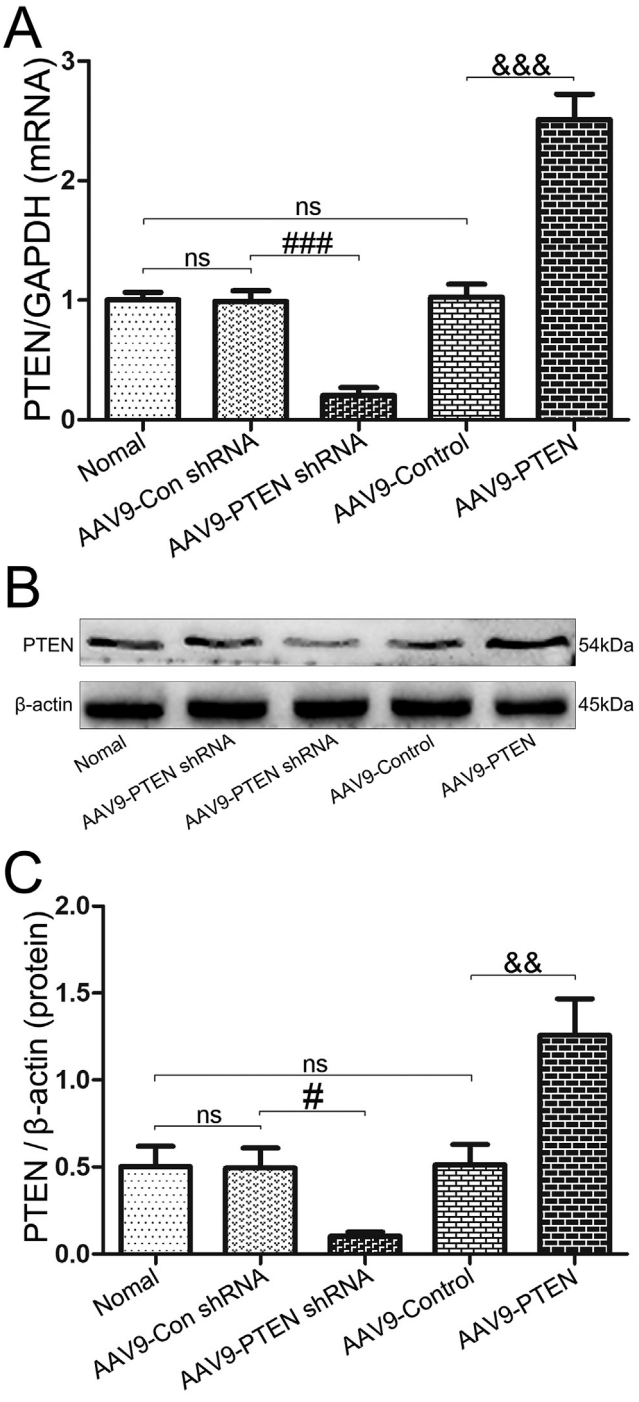

Figure 4 PTEN expression could be effectively suppressed or stimulated by adeno-associated virus injected into the lateral ventricle. **(A)** mRNA expression of PTEN after adeno-associated virus injection. **(B)** Protein expression of PTEN after adeno-associated virus injection. **(C)** Quantitative analysis of PTEN. Data represent the mean ± SD ($n = 5$ per group). ($^{\#}P$ *or* $^{\&}P<0.05$, $^{\#\#}P$ *or* $^{\&\&}P<0.01$, *vs.* $^{\#\#\#}P$ *or* $^{\&\&\&}P<0.001$, # means compared with the AAV9-Con shRNA group; & means compared with the AAV9-Control group; ns means no statistical difference).

manufacturer's instructions. Three slides of each rat were TUNEL stained, images were obtained from 3 fields of view of each slide, and TUNEL-positive cells were counted in the cortical area. After TUNEL staining, the nuclei were labeled with DAPI. A negative control was created using a labeled solution instead of the TUNEL reaction mixture. Data are expressed as the number of TUNEL-positive neurons per total number of neurons. TUNEL staining was performed in five brains.

Western blot analysis

Samples of rat cortical brain tissue were collected for total protein extraction, and the protein concentration was measured using an enhanced BCA protein assay kit (P0010, Beyotime Biotechnology, Jiangsu, China). Equal amounts of protein were denatured in SDS and separated on a 10% SDS-PAGE gel. The protein was transferred to a polyvinylidene fluoride (PVDF) membrane by electrophoresis and electrophoresis. The membrane was blocked with 5% milk and incubated with the primary antibody overnight at 4 °C, including β-APP (ab32136, 1:1000, Abcam, Cambridge, MA, USA), Bcl-2 (#15071, 1:1000, CST, Danvers, MA, USA), Bax (#5023, 1:1000, CST, Danvers, MA, USA), Phospho-PTEN (#9551, 1:1000, CST, Danvers, MA, USA), PTEN (ab79156, 1:1000, Abcam, Cambridge, MA, USA), Phospho-AKT (#4060, 1:2000, CST, Danvers, MA, USA), AKT (#9272, 1:1000, CST, Danvers, MA, USA), Phospho-GSK-3β (#5558, 1:1000, CST, Danvers, MA, USA), GSK-3β (#12456, 1:1000, CST, Danvers, MA, USA), Phospho-CRMP-2 (#9397, 1:1000, CST, Danvers, MA, USA), CRMP-2 (#9393, 1:1000, CST, Danvers, MA, USA), and β-actin (#4970, 1:1000, CST, Danvers, MA, USA). Then, they were incubated with HRP-labeled Goat Anti-Rabbit IgG (H + L) (A0208, 1:1000, Beyotime, Shanghai, China) and HRP-labeled Goat Anti-Mouse IgG (H + L) (A0216, 1: 1000, Beyotime, Shanghai, China) at 37 °C for 2 h and then developed by BeyoECL Plus chemiluminescence. Images were collected by the Bio-Rad gel imaging system, and the bands were quantified using Quantity One software. β-actin was set as the internal reference. The experiments were performed in triplicate.

Statistical analysis

All statistical analyses were performed using SPSS software 19.0 (IBM, USA). Values are expressed as the mean ± standard deviation. Data were analyzed using a one-way ANOVA followed by Tukey's HSD post hoc test and the Holm-Bonferroni correction. The remaining data were analyzed by Student's *t* test. A value of $P < 0.05$ was considered statistically significant. A nonparametric analysis of variance was used for categorical variables.

Results

SAH grade and mortality

SAH severity scores were determined in the experimental group, and the mean SAH score was 13.21 ± 1.98. There

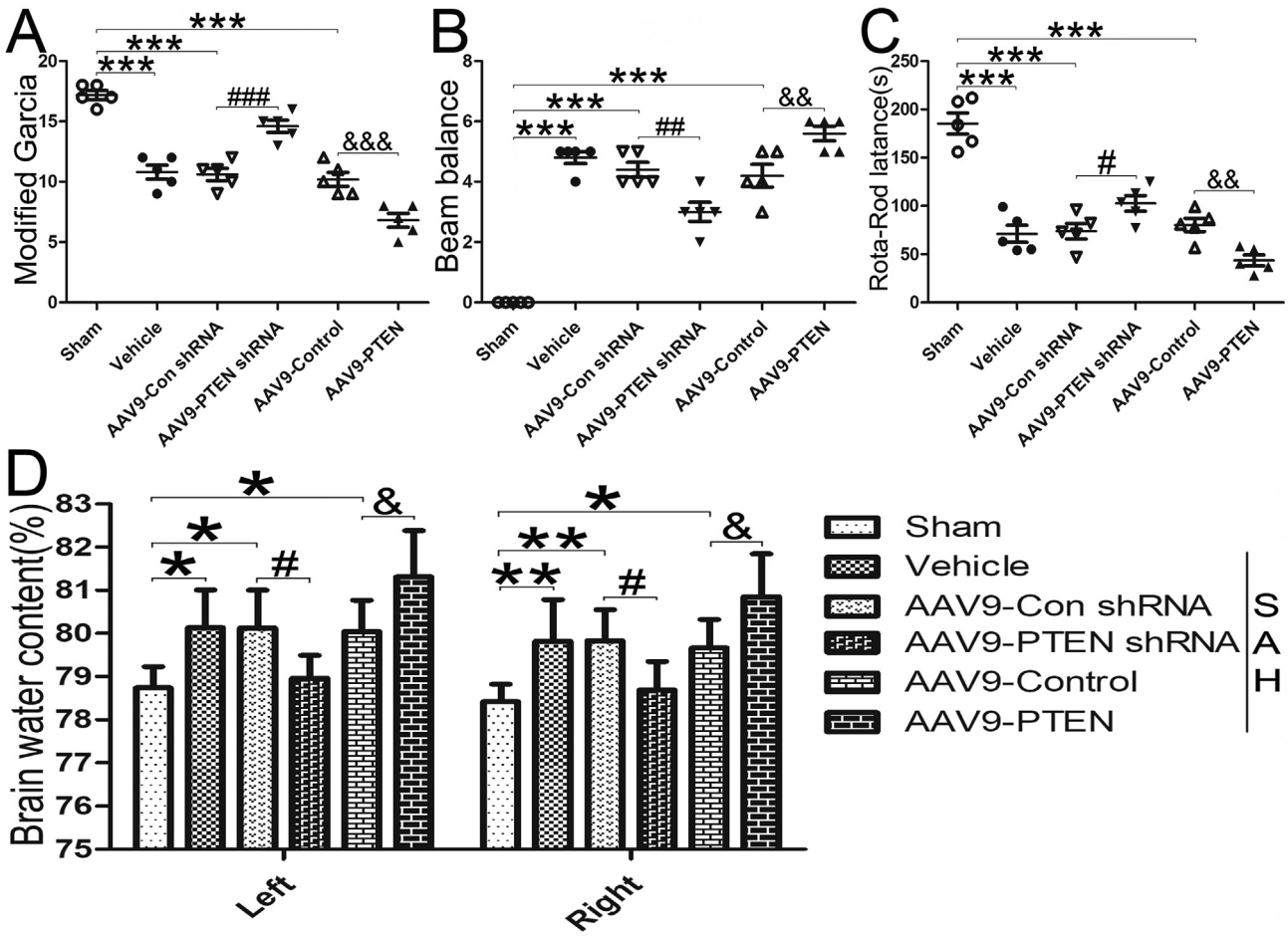

Figure 5 Neural function and brain tissue water content were improved by PTEN shRNA 24 h after SAH in rats, and overexpression of PTEN reversed these results. (**A**) Modified Garcia neurological function score. (**B**) Balance beam experiment. (**C**) Rotating rod experiment. (**D**) Brain water content. Data represent the mean ± SD ($n = 5$ per group). (*P,$^{\#}P$ or $^{\&}P<0.05$, **P,$^{\#\#}P$ or $^{\&\&}P<0.01$, *vs.* ***P,$^{\#\#\#}P$ or $^{\&\&\&}P<0.001$, * means compared with the sham group; # means compared with the AAV9-Con shRNA group; & means compared with the AAV9-Control group).

were no significant differences in severity scores between groups ($P > 0.05$) (Fig. 1D).

Mortality rates in experimental groups (Table 1). The overall mortality of SAH rats was 16.07% (36 of 224).

SAH increased PTEN, β-APP, and bax and decreased p-PTEN and Bcl-2 in the left cortex, with the most significant changes observed at 24 h

To elucidate the changes in PTEN after SAH and whether axons were damaged and neurons experienced apoptosis, the PTEN mRNA and protein as well as β-APP, Bcl-2 and Bax protein were detected. Compared with the sham group, PTEN mRNA (5.947 ± 0.975 *vs.* 0.989 ± 0.489, $P = 0.000 < 0.001$, Fig. 2A) and protein (0.952 ± 0.272 *vs.* 0.235 ± 0.153, $P = 0.000 < 0.001$, Fig. 2B, C) peaked at 24 h after SAH. Compared with the sham group, the phosphorylation of PTEN reached the minimum at 24 h (0.346 ± 0.190 *vs.* 1.801 ± 0.311, $P = 0.000 < 0.001$, Fig. 2B, D). β-APP continued to rise within 72 h after the emergence of SAH, which could begin as early as 3 h and reached a peak at 24 h compared with the sham group (0.932 ± 0.284 *vs.* 0.117 ± 0.097, $P = 0.000 < 0.001$, Fig. 2B, E). The expression of Bcl-2 gradually decreased, compared with the sham group, it reached the lowest value at 24 h (0.176 ± 0.133 *vs.* 1.028 ± 0.228, $P = 0.000 < 0.001$, Fig. 2B, F). The expression of Bax was opposite to that of Bcl-2 and reached a peak at 24 h compared with the sham group (0.819 ± 0.174 *vs.* 0.123 ± 0.079, $P = 0.000 < 0.001$, Fig. 2B, G). According to the characteristics of the time course, our subsequent experiments were observed at 24 h after SAH.

PTEN expression increased in the cortex and subcortical WM regions after SAH

The immunofluorescence analysis showed that PTEN was expressed in the cortex and subcortical WM regions and co-localized with β-III tubulin 24 h after SAH, compared with the sham operation group, the expression of PTEN in cell bodies and axons of neurons was significantly increased (57.135 ± 6.440% *vs.* 35.653 ± 5.193%, $P = 0.001 < 0.01$, Fig. 3A, B). In addition, we also observed the expression of

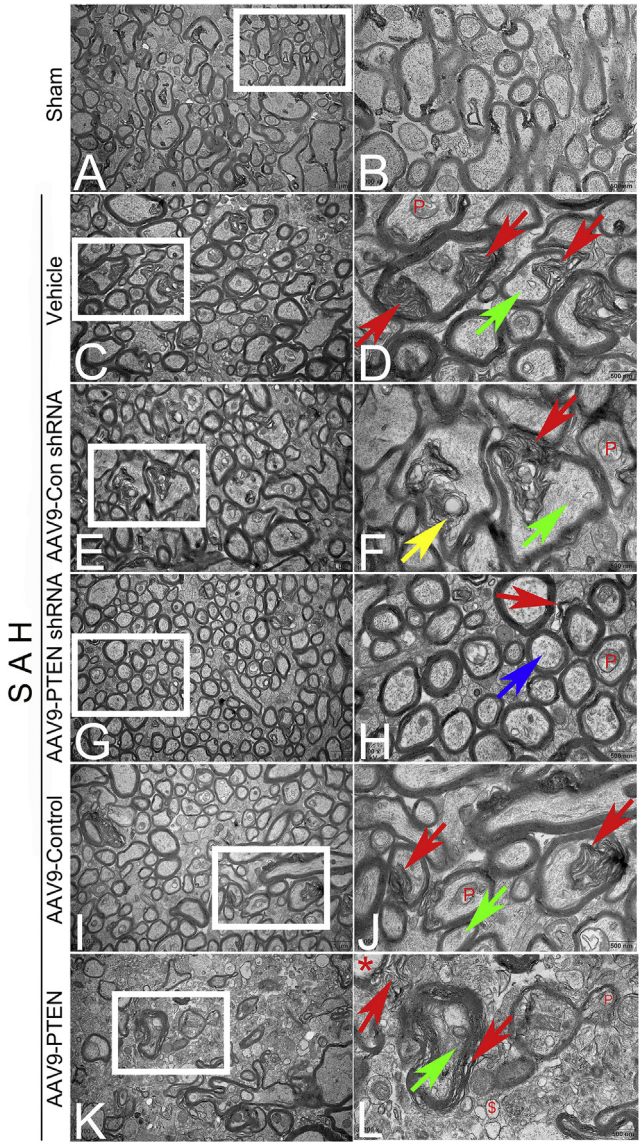

Figure 6 Changes in axon ultrastructure at 24 h after SAH. **(A, B)** In the sham operation group, the myelinated fibers and non-myelinated fibers were evenly distributed, the axons showed slight swelling and the myelin sheath, mitochondria, and microfilaments and microtubules were intact. **(C—F, I, J)** In the vehicle, AAV9-Con shRNA and AAV9-Control groups, the unmyelinated fibers were greatly reduced, the axonal diameter was enlarged, and the shape became irregular. Mitochondrial swelling (red P), myelin sheath disorder, delamination, inversion, thinning (red arrow), dense filaments (green arrow), myeloid changes in mitochondria (yellow arrow). **(G, H)** In the AAV9-PTEN shRNA group, myelinated fibers and unmyelinated fibers were more evenly distributed but had different degrees of swelling. The axle diameter was basically normal, and it was regular round or oval. Mitochondrial swelling (red P), local eversion disorder of the myelin sheath (red arrow), and microtubules still intact (blue arrow). **(K, L)** In the AAV9-PTEN group, the number of axons was reduced, and the axon shapes were irregular and accompanied by severe swelling. Axons were stacked and the microtubules disintegrate (red *), mitochondria were swollen (red P), myelinated fibers were swollen and damaged (red $), myelin was very disordered, layered, inwardly folded, thinned, and partially disintegrated (red arrow), and nerve filaments were densely packed (green arrow). ($n = 5$ per group); (left) Scale bar = 1 μm (12000×); (right) Scale bar = 500 nm (30000×).

PTEN in astrocytes and microglia, and the results were negative (data not shown).

qRT-PCR and WB confirm that PTEN expression could be effectively suppressed or stimulated by adeno-associated virus injected into the lateral ventricle

After adeno-associated virus was injected into the lateral ventricle of rats, the expression of PTEN in the subcortical WM region was significantly suppressed or stimulated. Regarding PTEN mRNA expression, compared with the AAV9-Con shRNA group, the AAV9-PTEN shRNA group was significantly decreased (0.203 ± 0.129 *vs.* 0.991 ± 0.178, $P = 0.000 < 0.001$, Fig. 4A). Compared with the AAV9-Control group, the AAV9-PTEN group was significantly increased (2.512 ± 0.421 *vs.* 1.027 ± 0.212, $P = 0.000 < 0.001$, Fig. 4A). Regarding PTEN protein expression, compared with the AAV9-Con shRNA group, the AAV9-PTEN shRNA group was significantly decreased (0.102 ± 0.047 *vs.* 0.494 ± 0.230, $P = 0.046 < 0.05$, Fig. 4B, C). Compared with the AAV9-Control group, the AAV9-PTEN group was significantly increased (1.257 ± 0.420 *vs.* 0.513 ± 0.233, $P = 0.001 < 0.01$, Fig. 4B, C).

Neurobehavioral function and cerebral edema in rats after SAH could be improved by knocking down PTEN, and overexpression of PTEN reversed these results

To explore the effects of PTEN on neurological function in rats after SAH, modified Garcia neurological function scores, balance beam experiments, and rotating rod experiments were used. Knocking down PTEN significantly increased the modified Garcia score compared with the AAV9-Con shRNA group (14.600 ± 1.140 *vs.* 10.600 ± 1.140, $P = 0.000 < 0.001$, Fig. 5A), whereas the overexpression of PTEN that reduced the score compared with the AAV9-Control group (7.000 ± 1.000 *vs.* 10.200 ± 1.304; $P = 0.000 < 0.001$, Fig. 5A). Rat performance on the balance beam was improved by knocking down PTEN compared with the AAV9-Con shRNA group (3.000 ± 0.707 *vs.* 4.400 ± 0.548, $P = 0.001 < 0.01$, Fig. 5B), but overexpression of PTEN resulted in a significant increase in the equilibrium beam score compared with the AAV9-Control group (5.600 ± 0.548 *vs.* 4.200 ± 0.837, $P = 0.001 < 0.01$, Fig. 5B). Rod time was significantly increased by knocking down PTEN compared with the AAV9-Con shRNA group (102.600 ± 18.311 *vs.* 73.800 ± 17.936, $P = 0.021 < 0.05$, Fig. 5C), while it was reduced by overexpression of PTEN compared with the AAV9-Control group (43.600 ± 12.621 *vs.* 80.400 ± 15.356, $P = 0.004 < 0.01$, Fig. 5C).

The water content of rat brain tissue was measured by wet and dry method. The brain water content in the left

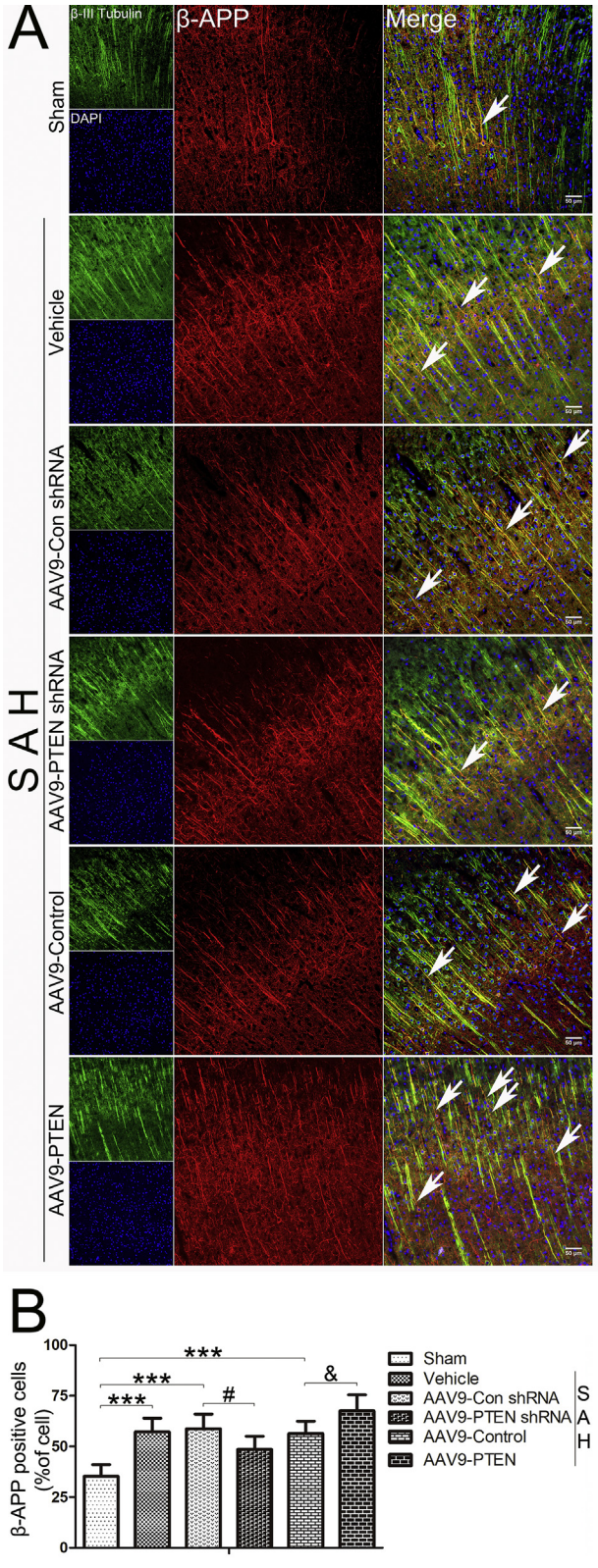

Figure 7 Axonal injury was reduced by PTEN shRNA after SAH in rats, and overexpression of PTEN aggravated this injury. **(A)** Expression of β-APP in the cortex and subcortical WM regions. **(B)** β-APP positive cell rate statistics. Data represent the mean ± SD ($n = 5$ per group). (*P,$^{\#}$P or $^{\&}P<0.05$, **P,$^{\#\#}$P or $^{\&\&}P<0.01$, *vs.* ***P,$^{\#\#\#}$P or $^{\&\&\&}P<0.001$, * means compared with the sham group; # means compared with the AAV9-Con shRNA group; & means compared with the AAV9-Control group). Scale bars = 50 μm.

and right hemispheres could be reduced by knocking down PTEN compared with the AAV9-Con shRNA group (left, 78.966 ± 0.524% *vs.* 80.125 ± 0.876%, $P = 0.029 < 0.05$; right, 78.690 ± 0.663% *vs.* 79.832 ± 0.716%, $P = 0.026 < 0.05$; Fig. 5D), while PTEN overexpression aggravates left and right brain hemisphere cerebral edema compared with the vehicle group (left, 81.310 ± 1.076% *vs.* 80.046 ± 0.726%, $P = 0.018 < 0.05$; right, 80.847 ± 0.993% *vs.* 79.662 ± 0.659%, $P = 0.021 < 0.05$; Fig. 5D).

Knocking down PTEN can reduce the degree of ultrastructural damage of axons after SAH, while overexpression of PTEN makes the damage worse

The ultrastructural changes of the axons after SAH were observed by transmission electron microscopy. Compared with the sham group, the axonal injury in the vehicle group after SAH was severe and the unmyelinated fibers were greatly reduced. The axon appeared swollen in the cross section, which was round; the myelin sheath became thin; the myelin sheaths were disordered, layered, inwardly folded, thinned; the mitochondria were swollen; the nerve filaments were densely packed; and the mitochondria appeared to show myeloid changes, which lead to energy metabolism disorders. In addition, the axons were not transported normally, and nerve electrical signal transmissions were blocked (Fig. 6C, D). When PTEN was knocked down, the myelinated fibers and unmyelinated fibers were distributed more evenly, the axons were protected, the myelin sheath was only partially damaged, and the microtubules and nerve filaments were less damaged (Fig. 6G, H). However, overexpression of PTEN significantly reduced axon density after SAH, swelling and destruction of myelinated nerve fibers, axonal swelling and even irregular shape, axillary pulp accumulation and microtubule disintegration, myelin layering was disordered, and even rupture and disintegration occurred, and axonal injury was very serious (Fig. 6K, L).

Axonal injury caused by SAH in rats could be reduced by knocking down PTEN and exacerbated by overexpression of PTEN

To understand the effect of PTEN on axonal injury in the cortex and subcortical WM regions of rats after SAH, we detected the protein expression of β-APP after intervention with PTEN. Neuronal cell bodies and axons could be localized and quantified by β-III Tubulin. The degree of axonal injury could be reflected by the ratio of β-APP positive cells. Immunofluorescence revealed that knockdown of PTEN could effectively reduce β-APP expression compared with the AAV9-Con shRNA group (48.575 ± 6.497% *vs.* 58.693 ± 7.289%, $P = 0.045 < 0.05$, Fig. 7A, B). In contrast, β-APP expression was significantly upregulated by PTEN overexpression compared with the AAV9-Control group (67.530 ± 7.939% *vs.* 56.393 ± 6.025%, $P = 0.028 < 0.05$, Fig. 7A, B).

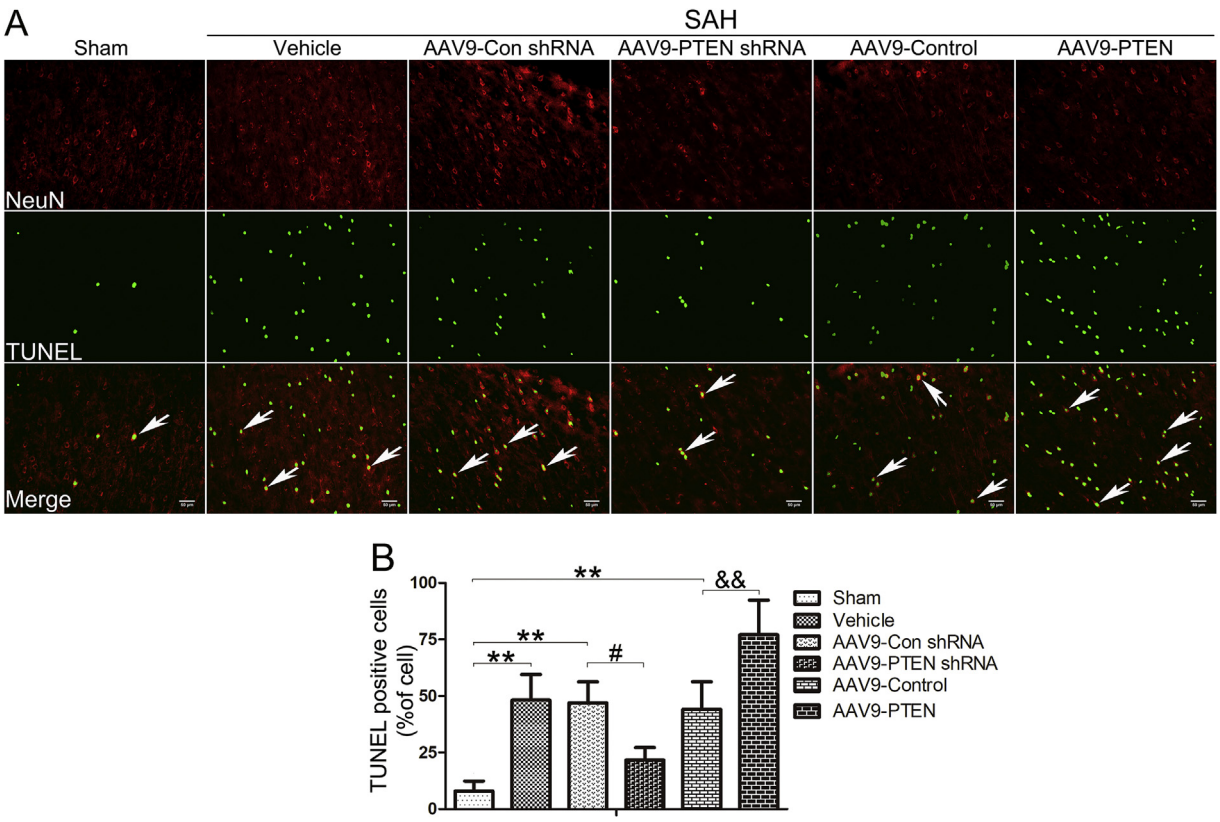

Figure 8 Neuronal apoptosis in rat cortical brain tissue caused by SAH was reduced by PTEN shRNA, and this apoptosis was significantly increased by overexpression of PTEN. **(A)** Immunofluorescence showed the TUNEL + neurons. **(B)** TUNEL-positive cell rate statistics. Data represent the mean ± SD ($n = 5$ per group). (*P,#P or &P<0.05, **P,##P or &&P<0.01, *vs.* ***P,###P or &&&P<0.001, * means compared with the sham group; # means compared with the AAV9-Con shRNA group; & means compared with the AAV9-Control group). Scale bars = 50 μm.

Neuronal apoptosis in rat cortical brain tissue caused by SAH was reduced by PTEN shRNA and exacerbated by PTEN overexpression

The effects of PTEN on neuronal apoptosis were investigated by TUNEL staining. Compared with the AAV9-Con shRNA group, neuronal apoptosis was significantly reduced by knockdown PTEN (21.687 ± 5.516% *vs.* 46.932 ± 9.370%, $P = 0.032 < 0.05$, Fig. 8A, B). In contrast, neuronal apoptosis was significantly increased by overexpressing PTEN compared with the AAV9-Control group (77.111 ± 15.300% *vs.* 44.105 ± 12.160%, $P = 0.007 < 0.01$, Fig. 8A, B).

3.9 Phosphorylation of PTEN, AKT, and GSK-3β was enhanced, CRMP-2 phosphorylation was attenuated, β-APP was decreased, Bcl-2 was increased and Bax was decreased at 24 h after SAH by knocking down PTEN.

Western blotting showed that the phosphorylation of AKT in the SAH group was inhibited (vehicle compared with sham, 0.339 ± 0.212 *vs.* 0.792 ± 0.219, $P = 0.009 < 0.01$, Fig. 9A, D), followed by the phosphorylation of GSK-3β was inhibited (vehicle compared with sham, 0.316 ± 0.189 *vs.* 0.803 ± 0.211, $P = 0.004 < 0.01$, Fig. 9A, E), and the phosphorylation of CRMP-2 became active (vehicle compared with sham, 0.724 ± 0.198 *vs.* 0.165 ± 0.111, $P = 0.000 < 0.001$, Fig. 9A, F). After SAH, the expression of PTEN in axons decreased (AAV9-PTEN shRNA compared with AAV9-Con shRNA, 0.454 ± 0.223 *vs.* 0.950 ± 0.225, $P = 0.004 < 0.01$, Fig. 9A, B), the phosphorylation of PTEN increased (AAV9-PTEN shRNA compared with AAV9-Con shRNA, 1.254 ± 0.440 *vs.* 0.318 ± 0.172, $P = 0.002 < 0.01$, Fig. 9A, C), the phosphorylation of AKT increased (AAV9-PTEN shRNA compared with AAV9-Con shRNA, 0.691 ± 0.242 *vs.* 0.343 ± 0.191, $P = 0.037 < 0.05$, Fig. 9A, D), the phosphorylation of GSK-3β also increased (AAV9-PTEN shRNA compared with AAV9-Con shRNA, 0.691 ± 0.223 *vs.* 0.345 ± 0.194, $P = 0.029 < 0.05$, Fig. 9A, E), and the phosphorylation of CRMP-2 decreased (AAV9-PTEN shRNA compared with AAV9-Con shRNA, 0.195 ± 0.119 *vs.* 0.763 ± 0.189, $P = 0.000 < 0.001$, Fig. 9A, F), and as a result, β-APP expression decreased (AAV9-PTEN shRNA compared with AAV9-Con shRNA, 0.488 ± 0.222 *vs.* 0.933 ± 0.226, $P = 0.007 < 0.01$, Fig. 9A, G), Bcl-2 increased (AAV9-PTEN shRNA compared with AAV9-Con shRNA, 0.553 ± 0.177 *vs.* 0.248 ± 0.165, $P = 0.037 < 0.05$, Fig. 9A, H), and Bax expression decreased (AAV9-PTEN shRNA compared with AAV9-Con shRNA, 0.344 ± 0.176 *vs.* 0.926 ± 0.205, $P = 0.000 < 0.001$, Fig. 9A, I).

Phosphorylation of PTEN, AKT, and GSK-3β was attenuated, CRMP-2 phosphorylation was enhanced, β-APP was increased, Bcl-2 was decreased and bax was increased at 24 h after SAH by overexpressing PTEN

Western blot showed that after SAH, the expression of PTEN in axons increased (AAV9-PTEN compared with AAV9-Control, 1.877 ± 0.476 *vs.* 0.924 ± 0.220, $P = 0.000 < 0.001$, Fig. 10A, B), the phosphorylation of PTEN decreased (AAV9-PTEN compared with AAV9-Control, 0.078 ± 0.038 *vs.* 0.516 ± 0.222, $P = 0.047 < 0.05$, Fig. 10A, C), the phosphorylation of AKT decreased (AAV9-PTEN compared with AAV9-Control, 0.105 ± 0.049 *vs.* 0.425 ± 0.187, $P = 0.046 < 0.05$, Fig. 10A, D), the phosphorylation of GSK-3β also decreased (AAV9-PTEN compared with AAV9-Control, 0.112 ± 0.050 *vs.* 0.441 ± 0.186, $P = 0.041 < 0.05$, Fig. 10A, E), the phosphorylation of CRMP-2 increased (AAV9-PTEN compared with AAV9-Control, 0.946 ± 0.389 *vs.* 0.554 ± 0.235, $P = 0.049 < 0.05$, Fig. 10A, F), and as a result, β-APP expression increased (AAV9-PTEN compared with AAV9-Control, 1.344 ± 0.403 *vs.* 0.856 ± 0.293, $P = 0.029 < 0.05$, Fig. 10A, G), Bcl-2 decreased (AAV9-PTEN compared with AAV9-Control, 0.091 ± 0.045 *vs.* 0.397 ± 0.159, $P = 0.045 < 0.05$, Fig. 10A, H), and Bax expression increased (AAV9-PTEN compared with AAV9-Control, 1.246 ± 0.385 *vs.* 0.738 ± 0.277, $P = 0.020 < 0.05$, Fig. 10A, I).

Discussion

Axonal injury, as a common consequence of nervous system trauma, is one of the common early features of CNS disease and may cause irreversible neurological dysfunction.[33–35] Among various pathological events in EBI, neuronal apoptosis is considered an important phenomenon, which may explain the short-term and long-term prognosis of SAH.[36] However, to the best of our knowledge, few scholars have studied the relationship between axonal injury and apoptosis in EBI after SAH at the molecular and cellular levels.

Our research found that:

1. Within 72 h after SAH, the dephosphorylation of PTEN-Ser380 (the signal of PTEN activation[37]) was continuous and the expression of PTEN protein gradually increased and reached a peak at 24 h. This process was accompanied by axonal injury and neuronal apoptosis, and it was more obvious at 24 h. PTEN could lead to further impairment of neurobehavioral function and cerebral edema in rats after SAH.
2. After SAH, axonal injury appeared in the subcortical WM region. Electron microscopy showed abnormalities in the myelin sheath, axon membrane, mitochondria, and axon cytoskeleton, including disorders and dissolution of the myelin sheath structure. The number of microtubules was reduced or completely loss; nerve filament spacing shrank, dense clustering occurred; axonal membrane segment was separated from the inner layer of the myelin sheath to expand the axon and myelin space; and mitochondrial swelling occurred, and these changes in the axon were consistent with the literature.[38–40] After inhibiting PTEN, the degree of axonal injury was significantly reduced, and the increased expression of PTEN caused the axonal injury to become more serious and even decreased the axonal density. The neurocytoskeleton is an important subcellular structure that maintains the normal morphology, structure, and function of axons.[41] Ultrastructural studies have shown that axonal swelling was closely related to the breakdown of the axon's cytoskeleton, and maintaining the stability of the cytoskeleton was the key link to protect the neural structure.[39,42] There is evidence that the effects of PTEN not only exist in the cytoplasm but also in mitochondria.[43] The N-terminal extension of PTEN is located in the cytoplasm and mitochondria, and then cytochrome C oxidase is unable to maintain a low phosphorylation state (required by mitochondria), leading to mitochondrial structure destruction and dysfunction.[44] Therefore, we speculated that PTEN interferes with mitochondrial energy metabolism and causes rapid axonal transport obstacles and β-APP accumulation; on the other hand, PTEN caused the proteins that constitute the axon cytoskeleton to be destroyed, making the neural cytoskeleton unable to maintain stability; thus the axonal injury described above irreversibly collapsed.
3. After SAH, neurons located in the cortex initiate an apoptotic program, and inhibition of PTEN could effectively reduce neuronal apoptosis. Overexpression of PTEN could significantly accelerate neuronal apoptosis. In this study, the Bax gene is an apoptosis-promoting member of the bcl-2 gene family. Bcl-2 protein is known to form heterodimers with Bax protein *in vivo*, and the molar ratio of Bcl-2 to Bax determines whether to induce or inhibit apoptosis in several tissues and cells.[45,46] We observed that PTEN could increase neuronal apoptosis, increase Bax expression and decrease Bcl-2 expression, while Bcl-2 expression may be related to activating the caspase-3 apoptosis cascade.
4. PTEN is widely expressed in the CNS and preferentially in neurons,[47] and our work confirmed that it was mainly expressed in the cell bodies and axons of neurons. Some studies have shown that neuronal survival could be improved by downregulating PTEN activity,[48,49] which is consistent with our view. Akt signaling is necessary for neuron survival after trophic factor deprivation, oxidative stress, and ischemic injury.[50] When we knocked down the PTEN gene, the serine at position 380 of PTEN was phosphorylated and the expression of PTEN was suppressed, which caused activation of the AKT signaling pathway and the phosphorylation of serine at position 473 of AKT (p-AKT is the active form). Next, the Akt signaling pathway phosphorylated serine 9 at GSK-3β, which was resulted in the inhibition of GSK-3β activity (p-GSK-3β is an inactive form). GSK-3β is involved in neuronal microtubule dynamics, and GSK-3β inactivates CRMP-2 by threonine at position 514.[18] After phosphorylation, p-CRMP-2 can inhibit the extension of neurites and damage axons.[51] In our experiments, because the activity of GSK-3β was inhibited, p-CRMP-2 expression

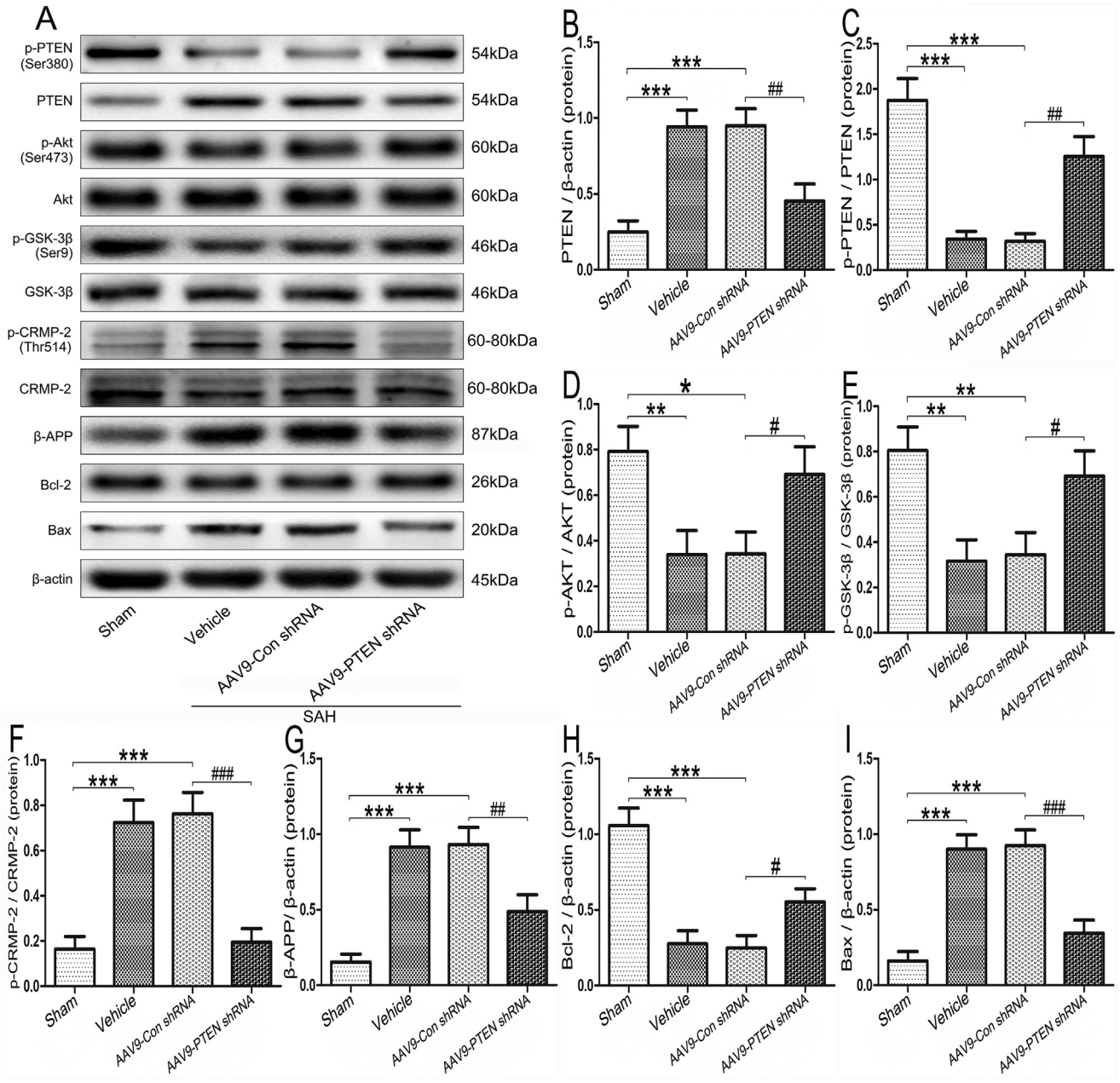

Figure 9 PTEN shRNA increased the amount of p-PTEN/p-AKT/p-GSK-3β/Bcl-2 and reduced the expression of PTEN/p-CRMP-2/β-APP/Bax in the left cortex at 24 h after SAH. **(A)** Western blot results. **(B—I)** Quantitative analysis of PTEN/(p-PTEN/PTEN)/(p-AKT/AKT)/(p-GSK-3β/GSK-3β)/(p-CRMP-2/CRMP-2)/β-APP/Bcl-2/Bax. Data represent the mean ± SD ($n = 5$ per group). (**P or #P*<0.05, ****P or ##P*<0.01, vs. *****P or ###P*<0.001,* means compared with the sham group; # means compared with the AAV9-Con shRNA group).

was reduced (p-CRMP-2 is an inactive form), which has a protective effect on axons. In addition, when PTEN was overexpressed, the AKT pathway was inhibited, and CRMP-2 was largely phosphorylated under the catalysis of activated GSK-3β. It was suggested that PTEN might aggravate neuronal axonal injury through inactivated CRMP-2-mediated microtubule disaggregation. In a study on diffuse axonal injury (DAI), during the formation of axonal globules after DAI, β-APP rapidly accumulated in the damaged transport area, and the tau complex might accumulate in tissues in the form of neurofibrillary tangles and subsequently trigger a large number of apoptosis.[52,53] Therefore, we speculated that in addition to deactivating the caspase-3 apoptosis cascade through Bcl-2 expression and increasing apoptosis in cortical neurons, PTEN and AKT/GSK-3β/CRMP-2 signaling pathway were involved in β-APP accumulation in axons, resulting in interruption of axonal plasma transport leading to increased neuronal apoptosis, and death of neurons caused by apoptosis will in turn aggravate axonal damage. It is this positive feedback mechanism that causes severe neurological deficits early after SAH.

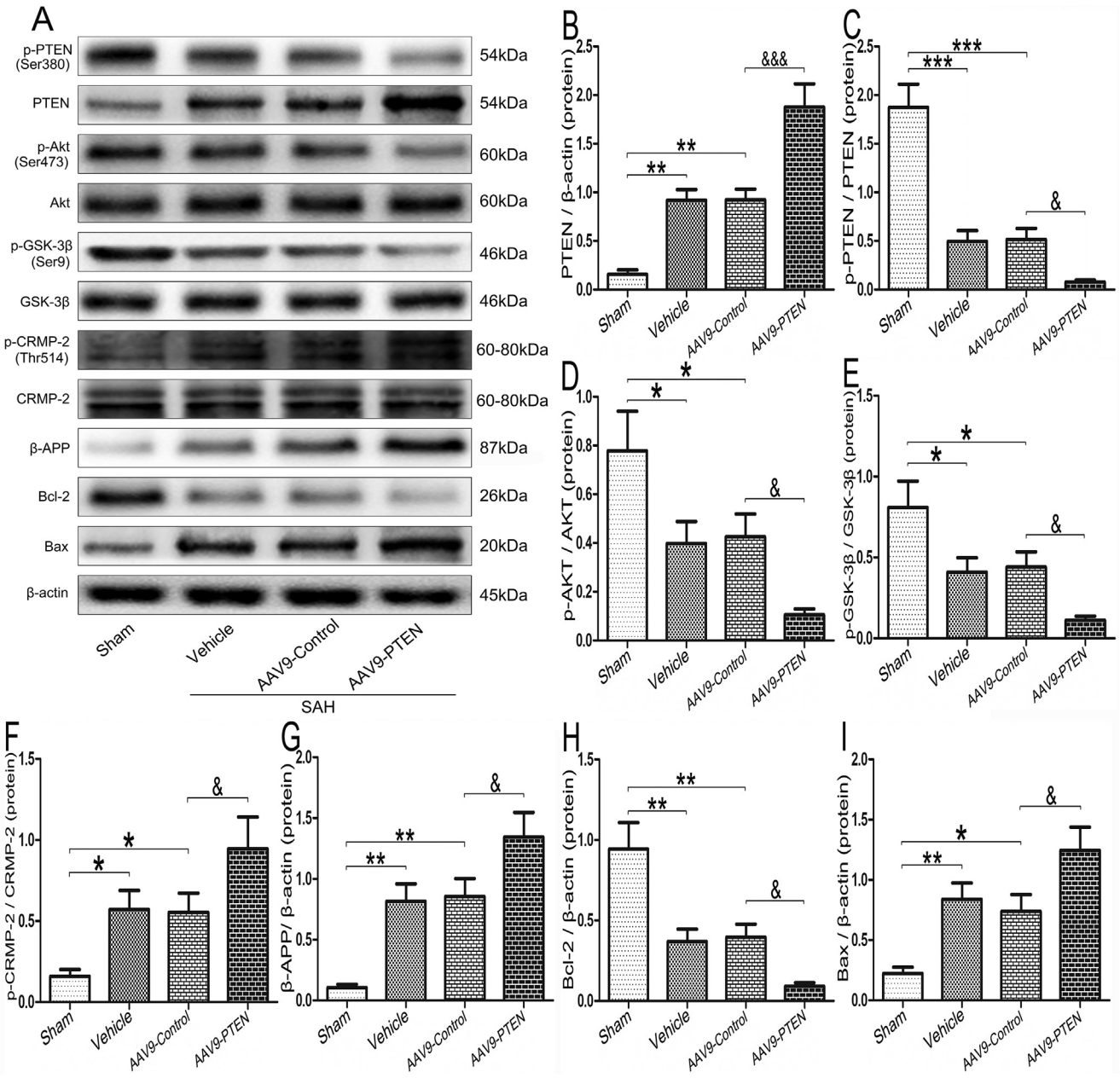

Figure 10 Over-expressing PTEN decreased the amount of p-PTEN/p-AKT/p-GSK-3β/Bcl-2 and increased the expression of PTEN/p-CRMP-2/β-APP/Bax in the left cortex at 24 h after SAH. **(A)** Western blot results. **(B—I)** Quantitative analysis of PTEN/(p-PTEN/PTEN)/(p-AKT/AKT)/(p-GSK-3β/GSK-3β)/(p-CRMP-2/CRMP-2)/β-APP/Bcl-2/Bax. Data represent the mean ± SD ($n = 5$ per group). (*P or $^{\&}P<0.05$, **P or $^{\&\&}P<0.01$, *vs.* ***P or $^{\&\&\&}P<0.001$,* means compared with the sham group; & means compared with the AAV9-Control group).

There are several shortcomings in our research. Firstly, we did not use PTEN inhibitors to intervene, such as dipotassium bisperoxo (pyridine-2-carboxyl) oxovanadate (BPV (pic)), a highly selective inhibitor of PTEN, and lost the opportunity to discuss drugs that target PTEN to improve SAH outcomes. Secondly, because we are focusing on EBI, we only observed a series of changes within 72 h after SAH. If we do not conduct research in a longer period, we will lose the opportunity to study axon repair and axon regeneration. Finally, we have only studied one pathway, PTEN/AKT/GSK-3β/CRMP-2. Although it was one of the most important and classic pathways in the AKT signaling pathway, any biological phenomenon must be a complex and comprehensive result. Therefore, there might be other signaling pathways involved in the regulation of neuronal apoptosis and axonal injury after SAH by PTEN. The above deficiencies will represent a direction of our next research study.

Conclusions

We demonstrated that PTEN expression increases after SAH. By PTEN gene silencing, WM axonal injury after SAH in rats was reduced, neuronal apoptosis was reduced,

cerebral edema was reduced, and neurobehavioral functions were improved. However, the overexpression of PTEN reversed the above results. PTEN may be involved in these effects with the AKT/GSK-3β/CRMP-2 signaling pathway. Therefore, these results suggest that the PTEN inhibition observed in this study may be a potential therapy to alleviate CNS damage (mainly referring to WM axon protection) and inhibit neuronal apoptosis after SAH to improve EBI.

Conflict of interests

The authors declare that there are no conflicts of interest.

Funding

This study was financially supported by the National Natural Science Foundation for Youth of China (No. 8160051302).

Appendix A. Supplementary data

Supplementary data to this article can be found online at https://doi.org/10.1016/j.gendis.2020.05.002.

References

1. Nieuwkamp DJ, Setz LE, Algra A, et al. Changes in case fatality of aneurysmal subarachnoid haemorrhage over time, according to age, sex, and region: a meta-analysis. *Lancet Neurol*. 2009;8(7):635—642.
2. Sehba FA, Hou J, Pluta RM, Zhang JH. The importance of early brain injury after subarachnoid hemorrhage. *Prog Neurobiol*. 2012;97(1):14—37.
3. Kou Z, Vandevord PJ. Traumatic white matter injury and glial activation: from basic science to clinics. *Glia*. 2014;62(11):1831—1855.
4. Koo EH, Sisodia SS, Archer DR, et al. Precursor of amyloid protein in Alzheimer disease undergoes fast anterograde axonal transport. *Proc Natl Acad Sci U S A*. 1990;87(4):1561—1565.
5. Mackenzie JM. Axonal injury in stroke: a forensic neuropathology perspective. *Am J Forensic Med Pathol*. 2015;36(3):172—175.
6. Sabri M, Kawashima A, Ai J, Macdonald RL. Neuronal and astrocytic apoptosis after subarachnoid hemorrhage: a possible cause for poor prognosis. *Brain Res*. 2008;1238:163—171.
7. Ding D, Starke RM, Dumont AS, et al. Therapeutic implications of estrogen for cerebral vasospasm and delayed cerebral ischemia induced by aneurysmal subarachnoid hemorrhage. *Biomed Res Int*. 2014;2014:727428.
8. Hopkins BD, Fine B, Steinbach N, et al. A secreted PTEN phosphatase that enters cells to alter signaling and survival. *Science*. 2013;341(6144):399—402.
9. Chen H, Xiang J, Wu J, et al. Expression patterns and role of PTEN in rat peripheral nerve development and injury. *Neurosci Lett*. 2018;676:78—84.
10. Christie KJ, Webber CA, Martinez JA, et al. PTEN inhibition to facilitate intrinsic regenerative outgrowth of adult peripheral axons. *J Neurosci*. 2010;30(27):9306—9315.
11. Li J, Lv H, Che YQ. Long non-coding RNA Gas5 potentiates the effects of microRNA-21 downregulation in response to ischaemic brain injury. *Neuroscience*. 2020;437:87—97.
12. Xiong T, Tang J, Zhao J, et al. Involvement of the Akt/GSK-3 beta/CRMP-2 pathway in axonal injury after hypoxic-ischemic brain damage in neonatal rat. *Neuroscience*. 2012;216:123—132.
13. Li B, Huang Z, Meng J, Yu W, Yang H. MiR-202-5p attenuates neurological deficits and neuronal injury in MCAO model rats and OGD-induced injury in Neuro-2a cells by targeting eIF4E-mediated induction of autophagy and inhibition of Akt/GSK-3 beta pathway. *Mol Cell Probes*. 2019:101497.
14. Frame S, Cohen P. GSK3 takes centre stage more than 20 years after its discovery. *Biochem J*. 2001;359(Pt 1):1—16.
15. Martin M, Rehani K, Jope RS, Michalek SM. Toll-like receptor-mediated cytokine production is differentially regulated by glycogen synthase kinase 3. *Nat Immunol*. 2005;6(8):777—784.
16. Inagaki N, Chihara K, Arimura N, et al. CRMP-2 induces axons in cultured hippocampal neurons. *Nat Neurosci*. 2001;4(8):781—782.
17. Shirvan A, Ziv I, Fleminger G, et al. Semaphorins as mediators of neuronal apoptosis. *J Neurochem*. 1999;73(3):961—971.
18. Mimura F, Yamagishi S, Arimura N, et al. Myelin-associated glycoprotein inhibits microtubule assembly by a Rho-kinase-dependent mechanism. *J Biol Chem*. 2006;281(23):15970—15979.
19. Jiang H, Guo W, Liang X, Rao Y. Both the establishment and the maintenance of neuronal polarity require active mechanisms: critical roles of GSK-3 beta and its upstream regulators. *Cell*. 2005;120(1):123—135.
20. Wakatsuki S, Saitoh F, Araki T. ZNRF1 promotes Wallerian degeneration by degrading AKT to induce GSK3B-dependent CRMP2 phosphorylation. *Nat Cell Biol*. 2011;13(12):1415—1423.
21. Duris K, Lipkova J, Splichal Z, Madaraszova T, Jurajda M. Early inflammatory response in the brain and anesthesia recovery time evaluation after experimental subarachnoid hemorrhage. *Transl Stroke Res*. 2019;10:308—318.
22. Takemoto Y, Hasegawa Y, Hayashi K, et al. The stabilization of central sympathetic nerve activation by renal denervation prevents cerebral vasospasm after subarachnoid hemorrhage in rats. *Transl Stroke Res*. 2020;11(3):528—540.
23. Chen R, McIntosh S, Hemby SE, et al. High and low doses of cocaine intake are differentially regulated by dopamine D2 receptors in the ventral tegmental area and the nucleus accumbens. *Neurosci Lett*. 2018;671:133—139.
24. Chen Q, Zhang J, Guo J, et al. Chronic hydrocephalus and perihematomal tissue injury developed in a rat model of intracerebral hemorrhage with ventricular extension. *Transl Stroke Res*. 2015;6(2):125—132.
25. Hayes MR, Skibicka KP, Leichner TM, et al. Endogenous leptin signaling in the caudal nucleus tractus solitarius and area postrema is required for energy balance regulation. *Cell Metab*. 2010;11(1):77—83.
26. Alhadeff AL, Mergler BD, Zimmer DJ, et al. Endogenous glucagon-like peptide-1 receptor signaling in the nucleus tractus solitarius is required for food intake control. *Neuropsychopharmacology*. 2017;42(7):1471—1479.
27. Wang J, Zuo Y, Zhuang K, et al. Recombinant human milk fat globule-epidermal growth factor 8 attenuates microthrombosis after subarachnoid hemorrhage in rats. *J Stroke Cerebrovasc Dis*. 2020;29(3):104536.
28. Zhou J, Gu L, Peng JH, et al. Expression of translocator protein in early brain injury after subarachnoid hemorrhage in mice. *Sichuan Da Xue Xue Bao Yi Xue Ban*. 2019;50(4):500—505.
29. Al-Afif S, Krauss JK, Helms F, et al. Long-term impairment of social behavior, vocalizations and motor activity induced by bilateral lesions of the fastigial nucleus in juvenile rats. *Brain Struct Funct*. 2019;224(5):1739—1751.
30. Lee D, Kim YS, Song J, Kim H. Neuroprotective Effects of Musk of Muskrat on Transient Focal Cerebral Ischemia in Rats. 2019;2019:9817949.

31. Song SH, Jee YS, Ko IG, et al. Treadmill exercise and wheel exercise improve motor function by suppressing apoptotic neuronal cell death in brain inflammation rats. *J Exerc Rehabil*. 2018;14(6):911—919.
32. Zhu H, Wang Y, Yang X, et al. Catalpol improves axonal outgrowth and reinnervation of injured sciatic nerve by activating Akt/mTOR pathway and regulating BDNF and PTEN expression. *Am J Transl Res*. 2019;11(3):1311—1326.
33. Schwab ME, Bartholdi D. Degeneration and regeneration of axons in the lesioned spinal cord. *Physiol Rev*. 1996;76(2):319—370.
34. Goldberg JL, Klassen MP, Hua Y, Barres BA. Amacrine-signaled loss of intrinsic axon growth ability by retinal ganglion cells. *Science*. 2002;296(5574):1860—1864.
35. Fitch MT, Silver J. CNS injury, glial scars, and inflammation: inhibitory extracellular matrices and regeneration failure. *Exp Neurol*. 2008;209(2):294—301.
36. Chen J, Wang L, Wu C, et al. Melatonin-enhanced autophagy protects against neural apoptosis via a mitochondrial pathway in early brain injury following a subarachnoid hemorrhage. *J Pineal Res*. 2014;56(1):12—19.
37. Zhang QG, Wu DN, Han D, Zhang GY. Critical role of PTEN in the coupling between PI3K/Akt and JNK1/2 signaling in ischemic brain injury. *FEBS Lett*. 2007;581(3):495—505.
38. Jafari SS, Maxwell WL, Neilson M, Graham DI. Axonal cytoskeletal changes after non-disruptive axonal injury. *J Neurocytol*. 1997;26(4):207—221.
39. Maxwell WL, Povlishock JT, Graham DL. A mechanistic analysis of nondisruptive axonal injury: a review. *J Neurotrauma*. 1997;14(7):419—440.
40. Jafari SS, Nielson M, Graham DI, Maxwell WL. Axonal cytoskeletal changes after nondisruptive axonal injury. II. Intermediate sized axons. *J Neurotrauma*. 1998;15(11):955—966.
41. Beazely MA, Lim A, Li H, et al. Platelet-derived growth factor selectively inhibits NR2B-containing N-methyl-D-aspartate receptors in CA1 hippocampal neurons. *J Biol Chem*. 2009;284(12):8054—8063.
42. Stoler O, Fleidervish IA. Functional implications of axon initial segment cytoskeletal disruption in stroke. *Acta Pharmacol Sin*. 2016;37(1):75—81.
43. Kreis P, Leondaritis G, Lieberam I, Eickholt BJ. Subcellular targeting and dynamic regulation of PTEN: implications for neuronal cells and neurological disorders. *Front Mol Neurosci*. 2014;7:23.
44. Liang H, He S, Yang J, et al. PTENα, a PTEN isoform translated through alternative initiation, regulates mitochondrial function and energy metabolism. *Cell Metab*. 2014;19(5):836—848.
45. Ola MS, Nawaz M, Ahsan H. Role of Bcl-2 family proteins and caspases in the regulation of apoptosis. *Mol Cell Biochem*. 2011;351(1—2):41—58.
46. Youle RJ, Strasser A. The BCL-2 protein family: opposing activities that mediate cell death. *Nat Rev Mol Cell Biol*. 2008;9(1):47—59.
47. Shrestha S, Yang K, Guy C, Vogel P, Neale G, Chi H. Treg cells require the phosphatase PTEN to restrain TH1 and TFH cell responses. *Nat Immunol*. 2015;16(2):178—187.
48. Choi YC, Lee JH, Hong KW, Lee KS. 17 Beta-estradiol prevents focal cerebral ischemic damages via activation of Akt and CREB in association with reduced PTEN phosphorylation in rats. *Fundam Clin Pharmacol*. 2004;18(5):547—557.
49. Delgado-esteban M, Martin-zanca D, Andres-martin L, Almeida A, Bolaños JP. Inhibition of PTEN by peroxynitrite activates the phosphoinositide-3-kinase/Akt neuroprotective signaling pathway. *J Neurochem*. 2007;102(1):194—205.
50. Noshita N, Lewén A, Sugawara T, et al. Akt phosphorylation and neuronal survival after traumatic brain injury in mice. *Neurobiol Dis*. 2002;9(3):294—304.
51. Ip JP, Fu AK, Ip NY. CRMP2: functional roles in neural development and therapeutic potential in neurological diseases. *Neuroscientist*. 2014;20(6):589—598.
52. Kaur B, Rutty GN, Timperley WR. The possible role of hypoxia in the formation of axonal bulbs. *J Clin Pathol*. 1999;52(3):203—209.
53. Zhao Y, Zhao Y, Zhang M, et al. Inhibition of TLR4 Signalling-Induced Inflammation Attenuates Secondary Injury after Diffuse Axonal Injury in Rats. *Mediators Inflamm*. 2016;2016:4706915.